

The VIMOS Public Extragalactic Redshift Survey (VIPERS). Unsupervised classification with photometric redshifts: a method to accurately classify large galaxy samples without spectroscopic information

M. Siudek^{1,2,3*}, K. Małek³, A. Pollo^{3,4}, B. R. Granett^{5,6}, M. Scodreggio⁷, T. Moutard^{8,9}, A. Iovino⁵, L. Guzzo^{6,5}, B. Garilli⁷, M. Bolzonella¹⁰, S. de la Torre⁹, U. Abbas¹¹, C. Adami⁹, D. Bottini⁷, A. Cappi^{10,12}, O. Cucciati¹⁰, I. Davidzon^{9,10}, P. Franzetti⁷, A. Fritz⁷, J. Krywult¹⁴, V. Le Brun⁹, O. Le Fèvre⁹, D. Maccagni⁷, F. Marulli^{13,15,10}, M. Polletta^{7,16,17}, L.A.M. Tasca⁹, R. Tojeiro¹⁸, D. Vergani¹⁰, A. Zanichelli¹⁹, S. Arnouts^{9,20}, J. Bel²¹, E. Branchini^{22,23,24}, J. Coupon²⁵, G. De Lucia²⁶, O. Ilbert⁹, L. Moscardini^{13,15,10}, G. Zamorani¹⁰, T. T. Takeuchi²⁷

(Affiliations can be found after the references)

Accepted XXX. Received YYY; in original form ZZZ

ABSTRACT

Techniques to classify galaxies solely based on photometry will be necessary for future large cosmology missions, such as Euclid or LSST. However, the precision of classification is always lower in photometric surveys and can be systematically biased with respect to classifications based upon spectroscopic data. We verified how precisely the detailed classification scheme introduced by Siudek et al. (2018, hereafter: S1) for galaxies at $z \sim 0.7$ could be reproduced if only photometric data are available. We applied the Fisher Expectation-Maximization (FEM) unsupervised clustering algorithm to 54,293 VIPERS galaxies working in a parameter space of reliable photometric redshifts and 12 corresponding rest-frame magnitudes. The FEM algorithm distinguishes four main groups: (1) red, (2) green, (3) blue, and (4) outliers. Each group is further divided into 3, 3, 4, and 2 subclasses, respectively. The accuracy of reproducing galaxy classes using spectroscopic data is high: 92%, 84%, 96% for red, green, and blue classes, respectively, except for dusty star-forming galaxies. The presented verification of the photometric classification demonstrates that large photometric samples can be used to distinguish different galaxy classes at $z > 0.5$ with an accuracy provided so far only by spectroscopic data except for particular galaxy classes.

Key words: galaxies: groups: general – galaxies: evolution – galaxies: star formation – galaxies: stellar content

1 INTRODUCTION

Nowadays it has become imperative to apply efficient classification tools to process large astronomical datasets. Forthcoming surveys, such as the European Space Agency’s Euclid mission (Laureijs et al. 2011) and the Large Synoptic Survey Telescope (Ivezic et al. 2008; LSST Science Collabo-

ration et al. 2009) will collect data on an unprecedented scale and will benefit from advancements in machine learning and deep learning techniques (see Fraix-Burnet et al. 2015 for a review). Machine learning methods have already proved to be successful in various astrophysical contexts, like discovering new exoplanets (e.g. Shallue & Vanderburg 2018), characterise quasars (e.g. Parks et al. 2018), distinguishing galaxy morphologies (e.g. Domínguez Sánchez et al. 2018) or deriving photometric redshifts (e.g. Bilicki et al. 2018).

* E-mail: msiudek@ifae.es

The upcoming datasets will allow unprecedented investigations into the physical processes underlying galaxy formation and evolution. A key step is to apply classification techniques to characterize the diversity of galaxy properties in order to infer the physical processes that drive the observed trends. Standard approaches to galaxy classification have relied on the bimodality in their colour distribution (e.g. Arnouts et al. 2013; Fritz et al. 2014; Haines et al. 2017; Krywult et al. 2017; Siudek et al. 2017). However, these approaches are incomplete in that they do not take advantage of all measurements available in the rich datasets. It has also been demonstrated that characterization based upon the bimodality can lead to systematic differences in the obtained properties depending on the selection criteria (e.g. Renzini 2006; Moresco et al. 2013).

New techniques adopted from the field of machine learning provide an alternative approach to classify galaxies effectively. Among the machine learning tools, of particular interest are clustering algorithms which partition the sample into groups. Broadly speaking, they can be separated into two main classes: supervised (when the classifier is trained with a representative sample) and unsupervised methods (without any training process). While supervised algorithms have demonstrated reasonable efficiency in automatic classification of unknown sources if a good training sample is provided (e.g. Solarz et al. 2012; Małek et al. 2013; Krakowski et al. 2016; Kurcz et al. 2016; Solarz et al. 2017), application of unsupervised machine learning techniques to galaxy classification is arguably yet to be proven. The advantage of unsupervised algorithms is that they can identify new classes of galaxies and interesting outliers in an objective manner. One of the challenges for unsupervised classifiers is the determination of the number of unique classes. Algorithms can merge classes with diverse properties or subdivide the distribution into too many unphysical classes and fail in following the continuous and physical nature of galaxy types (e.g. Sánchez Almeida et al. 2010; Hocking et al. 2018).

Unsupervised machine learning algorithms have so far been applied to classify spectroscopic galaxy measurements based on Principal Component Analysis (PCA) and k-means analysis (e.g. Sánchez Almeida et al. 2010; Marchetti et al. 2012; Peth et al. 2016). Using photometric data for classification purposes is less precise than with spectroscopic data due to larger errors. Unfortunately, obtaining full spectroscopic information in wide-field imaging surveys is not practical due to the large number of galaxies and high costs in observing time, especially for high-redshift sources. The next generation of extragalactic surveys will be dominated by multi-band photometry data. Therefore, there is a strong necessity to develop clustering tools able to provide galaxy classification using photometric redshift (hereafter z_{phot}) on a comparable accuracy level as when using spectroscopic redshift (hereafter z_{spec}).

In S1 we introduce a new approach to the galaxy classification based on the unsupervised Fisher Expectation-Maximization (hereafter FEM; Bouveyron & Brunet 2011) algorithm, which works in the multidimensional space of absolute magnitudes (in 12 different filters) and z_{spec} . The classification is thus based on a large parameter space, rather than just on the standard colour-colour plane, and therefore is more sensitive to the galaxy properties. The classification based upon broadband magnitudes allows detailed evolution

studies of the red sequence, blue cloud and green valley. The FEM algorithm separates different galaxy classes and determines the optimal number of homogeneous classes automatically, yielding 11 galaxy classes from the earliest to the latest types with an additional group of outliers (mainly broad-line AGNs observed at $z \sim 2$; S1). The galaxy sequence is reflected in their colours, but also their morphological, physical and spectroscopic properties which are not included in the classification scheme. In this paper we present the photometric classification (hereafter PHOT classification) of VIPERS galaxies and its comparison to the z_{spec} -based classification (hereafter SPEC classification; S1). The aim of the paper is to verify how precisely the SPEC classification can be reproduced by photometric data solely for a purpose of future surveys.

The paper is organized in the following way: In Sect. 2 we present the VIPERS data sample. Sect. 3 presents results and discusses their physical interpretation. The summary is presented in Sect. 4. Throughout this paper the cosmological framework assumes $\Omega_m = 0.30$, $\Omega_\Lambda = 0.70$, and $H_0 = 70 \text{ km s}^{-1} \text{ Mpc}^{-1}$.

2 DATA AND SAMPLE SELECTION

The analysis presented in this paper is based on the final galaxy sample from the VIMOS Public Extragalactic Redshift Survey (VIPERS, Scodreggio et al. 2018) performed with the VIMOS spectrograph mounted on the Very Large Telescope at ESO (VIMOS, Le Fèvre et al. 2003). VIPERS was designed to map the large-scale distribution of galaxies over an unprecedented volume of $5 \times 10^{-3} h^3 \text{ Mpc}^{-3}$ in the redshift range $0.5 < z < 1.2$. A simple and robust pre-selection in the ($u-g$) and ($r-i$) colour-colour plane was used to remove galaxies with $z < 0.5$ (Guzzo et al. 2014). VIPERS provided spectroscopic redshifts of 86,775 galaxies limited to $i_{AB} \leq 22.5$ mag over an area of $\sim 23.5 \text{ deg}^2$ and corresponding full photometrically-selected parent catalogue. The associated photometric catalogue consists of magnitudes based on u -, g -, r -, i - and z -band imaging from the CFHTLS T0007 release (Hudelot et al. 2012), FUV and NUV observations from GALEX (Martin et al. 2005), and new Ks -band observations conducted as part of the VIPERS Multi-Lambda Survey (VIPERS-MLS; Moutard et al. 2016a), complemented by Ks -band measurements from VIDEO (Jarvis et al. 2013). A detailed description of the VIPERS survey can be found in Guzzo et al. (2014) and Scodreggio et al. (2018).

In this paper, we present the classification based on the absolute magnitudes and z_{phot} . Similarly as in the SPEC classification (S1) the absolute magnitudes are derived by spectral energy distribution (SED) fitting described in Moutard et al. (2016b), except that now the computation is based on the z_{phot} from the VIPERS-MLS (for full description of z_{phot} measurements, please refer to Moutard et al. 2016a).

Our photometric sample includes the whole sample (52,113 objects) classified with the SPEC classification (sample selection is discussed by S1) completed by additional 2,180 sources. 2,148 sources of those 2,180 are spectroscopically confirmed stars, as such sources (on average $z_{phot} = 0.7$) are expected to contaminate photometrically selected samples. The remaining 32 sources are high-redshift objects

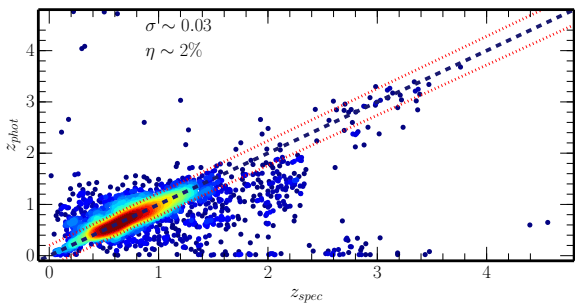


Figure 1. The comparison between z_{phot} and the corresponding z_{spec} of 54,293 VIPERS sources used in the following analysis. The blue dashed line corresponds to $z_{phot} = z_{spec}$. The red dotted lines show the threshold for defining outliers.

($z_{spec} > 1.5$) which are excluded from the spectroscopic sample defined in S1 as they are SED-fitting failures. Our sources cover the redshift range $0.3 < z_{phot} < 1.2$, reaching down to $z_{phot} \sim 0$ and up to $z_{phot} \sim 4.8$.

The comparison between z_{phot} and z_{spec} for the VIPERS sample is shown in Fig. 1. The measured scatter is $\sigma_{\delta z/(1+z)} \sim 0.03$ and the outlier rate¹ is $\eta \sim 2\%$.

3 RESULTS

3.1 The optimal class number

To verify the applicability of this galaxy classification method in the case of z_{phot} catalogues we applied for VIPERS photometric sample the same unsupervised algorithm as described in Siudek et al. (2018). The parameter space was constructed from 12 absolute magnitudes (normalised rest-frame to i band) and z_{phot} of VIPERS galaxies (in contrast to z_{spec} in Siudek et al. 2018). We ran the FEM algorithm on the PHOT sample based on the multidimensional space, and the optimal number of classes (12) and the best discriminative latent mixture (DLM) model (DBk) are established using the same approach as for SPEC classification (S1). We note that the optimal number of classes is the same as for SPEC classification; a new class of stars appears, but we are not able to distinguish one of the star-forming classes (namely, dusty star-forming galaxies from SPEC class 8 are merged with PHOT class 9; see Fig. 2 and 4) and so the number of classes is preserved. Both in the SPEC and PHOT classification process, the sources are not strictly assigned to one class, but the probability of being a member of each class is given. However, 94% of sources have their assignment well defined, i.e. have a high probability ($> 75\%$) of belonging to one class. In the following discussion we use only class members with a high probability of belonging to a given class, rejecting 3,007 objects with low class membership probability ($< 50\%$) or with a high

¹ Following Ilbert et al. (2006) and Moutard et al. (2016b) the scatter is defined as $\sigma_{\Delta z/(1+z)} = 1.48 \cdot \text{median}(|z_{spec} - z_{phot}|/(1+z_{spec}))$, and the photo-z outlier rate, η as the percentage of galaxies with $|\Delta z|/(1+z) > 0.15$.

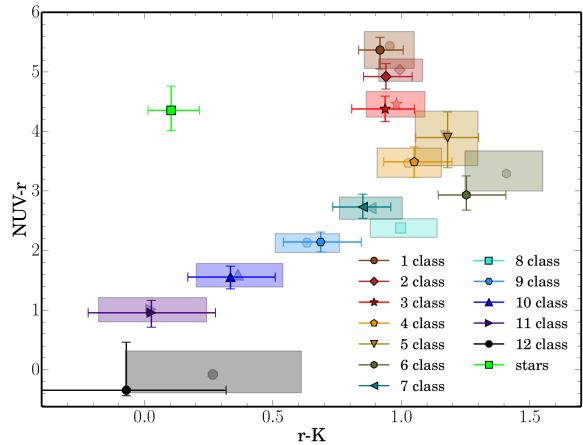


Figure 2. The $NUVrK$ diagram of the VIPERS galaxies classified into 12 classes according to the FEM algorithm using z_{phot} (points with error bars) and z_{spec} (rectangles). The error bars and size of squares correspond to the 25th, and 75th percentile range of the galaxy colour distribution. The median colours are marked with points.

($> 45\%$) probability of belonging to the second group (see S1 for details).

3.2 Galaxy class properties

The 12 different photometric classes (hereafter PHOT class) within the VIPERS sample follow the trend from red, passive, through green, intermediate, to blue, star-forming galaxy types, with an additional groups of outliers (stars and AGNs). Even if such a detailed classification is possible only in the full multidimensional parameter space, it is well reflected by the positions of groups on the $(NUV - r)$ vs. $(r - K)$ diagram (hereafter $NUVrK$, Arnouts et al. 2013) diagram². Fig. 2 presents a comparison of the distribution of the FEM classes in the $NUVrK$ diagram, when z_{phot} and z_{spec} were used in the classification procedure.

The galaxy sequence obtained from the PHOT classification almost exactly mirrors the spectroscopic classes (hereafter SPEC classes). Fig. 2 shows that the median $NUV - r$ and $r - K$ colours of red galaxies (classes 1–3) are similar in both classifications. Green galaxies (classes 4–6) are also located in the same area in the $NUVrK$ diagram in SPEC and PHOT classifications. The main difference is displayed by the group of star-forming galaxies. In the PHOT classification four star-forming galaxy classes are found, whereas in the SPEC classification five star-forming groups are distinguished. One additional class in SPEC classification (SPEC class 8) is characterized by redder rK colours ($r - K_{median} = 1.00^{+0.12}_{-0.14}$) and higher star formation rate (hereafter SFR ; $SFR = 1.41^{+0.28}_{-0.30}$) than the remaining star-forming classes. These galaxies are mostly assigned to the PHOT class 9 of star-forming galaxies ($\sim 75\%$;

² Note, however, that the three (NUV, r, K) parameter space would not be large enough to create such a fine division.

see also Fig. 4). This might be a consequence of the discrete nature of SED templates, which resulted in the lowest z_{phot} accuracy ($\sigma_{\delta z/(1+z)} \sim 0.037$) for galaxies within SPEC class 8 among all classes (except class 12) and yields the inability of distinguishing more dusty star-forming galaxies. We note that also in the SPEC classification those galaxies are not straightforwardly distinguished. Galaxies in SPEC class 8 are characterized by lower membership probability than other SPEC classes (see Fig. C.1 in S1). Moreover, the SPEC class 8 is distinguished on the last cycle of the FEM algorithm, i.e. the class is absent if we consider a SPEC classification with only 11 classes (Fig. B.2 and B.3 in S1). Extremely dusty green galaxies (class 6) are, however, properly identified in the PHOT classification (see Fig. 2 and 4).

Furthermore, in the PHOT classification an additional group of outliers (marked with green in Fig. 2) is separated. The class of outliers with red $NUV - r$ and blue $r - K$ colours is mainly (96%) composed of stars (not included in the original SPEC sample but added to the PHOT sample to model photometric data in a realistic way). More than half of the stars present in the photometric dataset (1,234 out of 2,148; 57%) are assigned to this class. The remaining 914 stars are distributed in different groups. However, they constitute just a small fraction of all members of the other classes except for class 12 (42%; 55 stars). Class 12, besides stars, consists of broad-line AGNs (50%). In the case of the SPEC classification it is a pure sample of broad-line AGNs (95%).

PHOT classification is able to recover the trends from SPEC classification in physically important parameters like line strength and morphology. Fig. 3 presents the comparison between the spectroscopic and morphological galaxy class properties: the strength of the 4000 break (D_{4000n} , as defined by Balogh et al. 1999), the equivalent widths for $[OII]\lambda 3727$, and the Sérsic index when z_{phot} and z_{spec} were used in the classification procedure are shown as a function of the class number. With the exception of SPEC class 8 (blue, dusty star-forming galaxies not distinguishable in the PHOT classification), the median properties of each class agree well in the two classifications and do not show any significant differences.

3.3 Statistical differences between spectroscopic and photometric classifications

Fig. 4 presents the distribution of VIPERS sources within SPEC classes (S1) and their migration to PHOT classes. The majority of objects ($> 70\%$) are assigned to the same class independently of the fact that z_{spec} or z_{phot} is used. However, a small "exchange" between classes occurred, mainly between classes located close to each other in the multidimensional feature space. For example PHOT class 2 (marked with dark red in Fig. 4) is built mainly from galaxies assigned to SPEC class 2 ($\sim 56\%$; dark red), but also includes objects from SPEC class 1 ($\sim 17\%$; brown), and 3 ($\sim 20\%$; red). There are also more extreme "jumping-objects" where sources assigned to e.g., red and passive SPEC classes are classified as intermediate or star-forming PHOT classes, and this is seen as thin flows between distant groups in Fig. 4. However, jumps over more than 2 neighbouring classes are very rare ($\sim 2\%$). Less secure assignment of these sources is also mirrored by their lower membership probability (mean probability for jumping-objects is lower by $\sim 7\%$ than those for members of

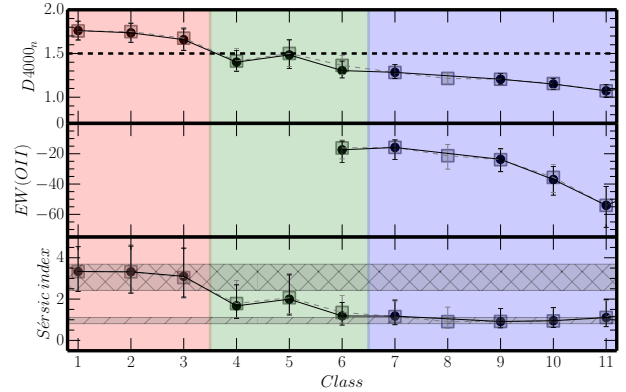


Figure 3. The distribution of the median values of D_{4000n} , $EW(OII)$, and Sérsic index for SPEC (marked with grey open squares) and PHOT (marked with black dots) classifications for red (classes 1–3), green (classes 4–6), star-forming (classes 7–11) galaxies are shown in red, green, and blue, respectively. The error bars correspond to 1st and 3rd quartile of the parameter distribution. The division between red passive and blue active galaxies based on D_{4000n} (Kauffmann et al. 2003) is marked with a black dashed line. The typical mean Sérsic index ranges for VIPERS red passive, and blue star-forming galaxies (Krywult et al. 2017) are marked with grey shadow areas. The $[OII]\lambda 3727$ line has not been detected in the majority of galaxies from SPEC and PHOT classes 1–5.

main streams). Therefore, some objects with a low PHOT membership probability do not migrate from the SPEC class to the corresponding PHOT class, but drastically change their classification. These galaxies are also characterized by lower z_{phot} accuracy ($\sigma_{\Delta z/(1+z)} \sim 0.05$), which may explain the difficulties in the assignment of the proper class.

4 CONCLUSIONS

We present an unsupervised classification of VIPERS sources observed at $z \sim 0.7$ based on the z_{phot} and corresponding absolute magnitudes. The unsupervised photometric classification does not require additional training with spectroscopic samples, after photometric redshifts have been estimated.

Three classes of red passive galaxies (classes 1–3) are correctly recovered if no spectroscopy information is provided (with an accuracy of 92%; see Tab. 1). Also green, intermediate galaxies (classes 4–6) are accurately (84%) separated when only z_{phot} is provided. Spectroscopy is also not necessary to separate blue, star-forming galaxies as a whole class, as the algorithm using z_{phot} is able to almost perfectly identify the same group as SPEC classification (96%). However, spectroscopic information is needed to obtain a more detailed picture of some of the blue subclasses. In particular, the PHOT classification is not able to separate dusty star-forming galaxies (SPEC class 8) from less dusty star-forming galaxies (class 9). This might be a consequence of the SED fitting procedure adapted to the VIPERS dataset (Moutard et al. 2016a), which is not able to describe properly dusty star-forming galaxies. Possibly, a better set of templates might improve the outcome. In the PHOT sample, which

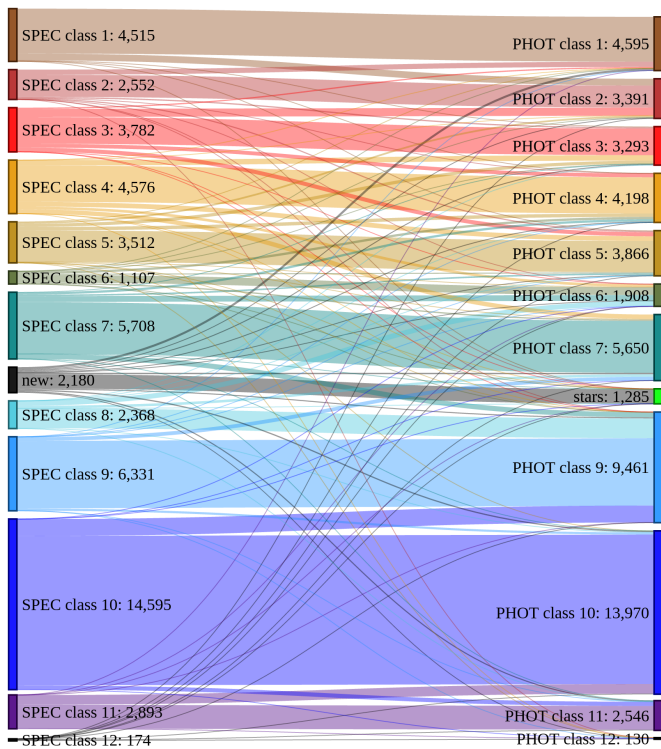


Figure 4. The distribution of 52,113 VIPERS galaxies and 2,180 additional sources (mainly stars) within 12 SPEC (left side) and PHOT classes (right side). The coloured lines show the correspondence between object assignments in the SPEC and PHOT classifications.

Cls	N_{spectro}	N_{photo}	A [%]	Cls	N_{spectro}	N_{photo}	A [%]
1	4,515	3,838	85	7	5,708	4,432	78
2	2,552	1,884	74	9	6,331	5,773	91
3	3,782	2,279	60	10	14,595	12,781	88
1-3	10,849	9,983	92	11	2,893	2,036	70
4	4,576	3,100	68	7-11	31,896	30,552	96
5	3,512	2,673	76	12	174	52	30
6	1,107	661	60				
4-6	9,195	7,662	84				

Table 1. The accuracy (A [%]) of the PHOT classification given as the percentage of the number of galaxies in each SPEC class (N_{spectro}) to the subsample of N_{spectro} galaxies which are found in the same PHOT class (N_{photo}).

includes stars, the algorithm, in some cases, is not able to distinguish stars and AGNs and, therefore, assigned them to the same class. This results in (expected) differences between PHOT class 12 and SPEC class 12. A detailed efficiency of the PHOT classification is given in Tab. 1.

We conclude that reliable z_{phot} ($\sigma \sim 0.03, \eta \sim 2\%$) allow for a highly effective identification of different galaxy classes at $z > 0.5$ by the FEM unsupervised algorithm. The resultant classification is almost identical with the classification based on z_{spec} , confirming that the FEM algorithm is a new robust tool, which can provide a detailed picture of galaxy types at $z \sim 0.7$ also without spectroscopic information. In general, it implies that for division into basic

blue/green/red classes at $z \sim 0.7$ the observed colours are sufficient and even incorrectly estimated redshifts do not affect the results significantly (especially the selection of red galaxies). However, for a finer division into subclasses, a correct redshift is necessary. To reproduce most subclasses the photometric accuracy as provided by our data is sufficient, except for blue dusty star-forming galaxies (SPEC class 8), where spectroscopic accuracy becomes crucial. The proper separation of this class, as well as broad-line AGNs and stars may depend on the accuracy of the SED templates of these objects. Overall, we have found that the purely photometric classification is not strongly biased with respect to the spectroscopic one. This excellent agreement gives us confidence that future photometric surveys can produce robust galaxy classifications useful for galaxy evolution studies.

ACKNOWLEDGEMENTS

VIPERS is based on observations collected at the European Southern Observatory, Cerro Paranal, Chile, using the Very Large Telescope under programs 182.A-0886 and partly 070.A-9007. Also based on observations obtained with MegaPrime/MegaCam, a joint project of CFHT and CEA/DAPNIA, at the Canada-France-Hawaii Telescope (CFHT), which is operated by the National Research Council (NRC) of Canada, the Institut National des Sciences de l’Univers of the Centre National de la Recherche Scientifique (CNRS) of France, and the University of Hawaii. This work is based in part on data products produced at TERAPIX and the Canadian Astronomy Data Centre as part of the Canada-France-Hawaii Telescope Legacy Survey, a collaborative project of NRC and CNRS. We acknowledge the crucial contribution of the ESO staff for the management of service observations. In particular, we are deeply grateful to M. Hilker for his constant help and support of this program. Italian participation in VIPERS has been funded by INAF through PRIN 2008, 2010, and 2014 programs. LG and BRG acknowledge support of the European Research Council through the Darklight ERC Advanced Research Grant (# 291521). OLF acknowledges support of the European Research Council through the EARLY ERC Advanced Research Grant (# 268107). KM, JK, MS have been supported by the National Science Centre (grant UMO-2013/09/D/ST9/04030). MS also acknowledges financial support from UMO-2016/23/N/ST9/02963 and AP from UMO-2017/26/A/ST9/00756 by the National Science Centre. RT acknowledge financial support from the European Research Council under the European Community’s Seventh Framework Programme (FP7/2007-2013)/ERC grant agreement n. 202686. EB, FM, and LM acknowledge the support from grants ASI-INAF I/023/12/0 and PRIN MIUR 2010-2011. LM also acknowledges financial support from PRIN INAF 2012.

REFERENCES

- Arnouts S., et al., 2013, *A&A*, **558**, A67
 Balogh M. L., Morris S. L., Yee H. K. C., Carlberg R. G., Ellingson E., 1999, *ApJ*, **527**, 54
 Bilicki M., et al., 2018, *A&A*, **616**, A69
 Bouveyron C., Brunet C., 2011, preprint ([arXiv:1101.2374](https://arxiv.org/abs/1101.2374))

- Domínguez Sánchez H., Huertas-Company M., Bernardi M., Tuccillo D., Fischer J. L., 2018, *MNRAS*, **476**, 3661
- Fraix-Burnet D., Thuillard M., Chattopadhyay A. K., 2015, *Frontiers in Astronomy and Space Sciences*, **2**, 3
- Fritz A., et al., 2014, *A&A*, **563**, A92
- George D., Huerta E. A., 2018, *Phys. Rev. D*, **97**, 044039
- Guzzo L., et al., 2014, *A&A*, **566**, A108
- Haines C. P., et al., 2017, *A&A*, **605**, A4
- Hocking A., Geach J. E., Sun Y., Davey N., 2018, *MNRAS*, **473**, 1108
- Hudelot P., et al., 2012, *VizieR Online Data Catalog*, **2317**
- Ilbert O., Arnouts S., McCracken H. J., et al., 2006, *A&A*, **457**, 841
- Ivezic Z., et al., 2008, preprint, ([arXiv:0805.2366](https://arxiv.org/abs/0805.2366))
- Jarvis M. J., et al., 2013, *MNRAS*, **428**, 1281
- Kauffmann G., et al., 2003, *MNRAS*, **341**, 33
- Krakowski T., Małek K., Bilicki M., Pollo A., Kurcz A., Krupa M., 2016, *A&A*, **596**, A39
- Krywult J., et al., 2017, *A&A*, **598**, A120
- Kurcz A., Bilicki M., Solarz A., Krupa M., Pollo A., Małek K., 2016, *A&A*, **592**, A25
- LSST Science Collaboration et al., 2009, preprint, ([arXiv:0912.0201](https://arxiv.org/abs/0912.0201))
- Laureijs R., et al., 2011, preprint, ([arXiv:1110.3193](https://arxiv.org/abs/1110.3193))
- Le Fèvre O., et al., 2003, in Iye M., Moorwood A. F. M., eds, *Society of Photo-Optical Instrumentation Engineers (SPIE) Conference Series Vol. 4841, Society of Photo-Optical Instrumentation Engineers (SPIE) Conference Series*. pp 1670–1681, [doi:10.1117/12.460959](https://doi.org/10.1117/12.460959)
- Małek K., et al., 2013, *A&A*, **557**, A16
- Marchetti A., et al., 2012, *MNRAS*, p. 107
- Martin D. C., et al., 2005, *ApJ*, **619**, L1
- Moresco M., et al., 2013, *A&A*, **558**, A61
- Moutard T., et al., 2016a, *A&A*, **590**, A102
- Moutard T., et al., 2016b, *A&A*, **590**, A103
- Parks D., Prochaska J. X., Dong S., Cai Z., 2018, *MNRAS*, **476**, 1151
- Peth M. A., et al., 2016, *MNRAS*, **458**, 963
- Renzini A., 2006, *ARA&A*, **44**, 141
- Sánchez Almeida J., Aguerri J. A. L., Muñoz-Tuñón C., de Vicente A., 2010, *ApJ*, **714**, 487
- Scodreggio M., et al., 2018, *A&A*, **609**, A84
- Shallue C. J., Vanderburg A., 2018, *AJ*, **155**, 94
- Siudek M., et al., 2017, *A&A*, **597**, A107
- Siudek M., et al., 2018, *A&A*, **617**, A70
- Solarz A., et al., 2012, *A&A*, **541**, A50
- Solarz A., Bilicki M., Gromadzki M., Pollo A., Durkalec A., Wypych M., 2017, *A&A*, **606**, A39
- ¹Institut de Física d'Altes Energies (IFAE), The Barcelona Institute of Science and Technology, 08193 Bellaterra (Barcelona), Spain
- ²Centre for Theoretical Physics, Al. Lotnikow 32/46, 02-668 Warsaw, Poland
- ³National Centre for Nuclear Research, ul. Hoza 69, 00-681 Warszawa, Poland
- ⁴Astronomical Observatory of the Jagiellonian University, Orla 171, 30-001 Cracow, Poland
- ⁵INAF - Osservatorio Astronomico di Brera, Via Brera 28, 20122 Milano – via E. Bianchi 46, 23807 Merate, Italy
- ⁶Università degli Studi di Milano, via G. Celoria 16, 20133 Milano, Italy
- ⁷INAF - Istituto di Astrofisica Spaziale e Fisica Cosmica Milano, via Bassini 15, 20133 Milano, Italy
- ⁸Department of Astronomy & Physics, Saint Mary's University, 923 Robie Street, Halifax, Nova Scotia, B3H 3C3, Canada
- ⁹Aix Marseille Univ, CNRS, LAM, Laboratoire d'Astrophysique de Marseille, Marseille, France
- ¹⁰INAF - Osservatorio di Astrofisica e Scienza dello Spazio di Bologna, via Gobetti 93/3, 40129 Bologna - Italy
- ¹¹INAF - Osservatorio Astrofisico di Torino, 10025 Pino Torinese, Italy
- ¹²Laboratoire Lagrange, UMR7293, Université de Nice Sophia Antipolis, CNRS, Observatoire de la Côte d'Azur, 06300 Nice, France
- ¹³Dipartimento di Fisica e Astronomia - Alma Mater Studiorum Università di Bologna, via Gobetti 93/2, I-40129, Bologna, Italy
- ¹⁴Institute of Physics, Jan Kochanowski University, ul. Swietokrzyska 15, 25-406 Kielce, Poland
- ¹⁵INFN, Sezione di Bologna, viale Berti Pichat 6/2, I-40127, Bologna, Italy
- ¹⁶IRAP, Université de Toulouse, CNRS, UPS, Toulouse, France
- ¹⁷IRAP, 9 av. du colonel Roche, BP 44346, F-31028 Toulouse cedex 4, France
- ¹⁸School of Physics and Astronomy, University of St Andrews, St Andrews KY16 9SS, UK
- ¹⁹INAF - Istituto di Radioastronomia, via Gobetti 101, I-40129, Bologna, Italy
- ²⁰Canada-France-Hawaii Telescope, 65–1238 Mamalahoa Highway, Kamuela, HI 96743, USA
- ²¹Aix Marseille Univ, Univ Toulon, CNRS, CPT, Marseille, France
- ²²Dipartimento di Matematica e Fisica, Università degli Studi Roma Tre, via della Vasca Navale 84, 00146 Roma, Italy
- ²³INFN, Sezione di Roma Tre, via della Vasca Navale 84, I-00146 Roma, Italy
- ²⁴INAF - Osservatorio Astronomico di Roma, via Frascati 33, I-00040 Monte Porzio Catone (RM), Italy
- ²⁵Department of Astronomy, University of Geneva, ch. d'Ecogia 16, 1290 Versoix, Switzerland
- ²⁶INAF - Osservatorio Astronomico di Trieste, via G. B. Tiepolo 11, 34143 Trieste, Italy
- ²⁷Division of Particle and Astrophysical Science, Nagoya University, Furo-cho, Chikusa-ku, 464-8602 Nagoya, Japan

This paper has been typeset from a $\text{\TeX}/\text{\LaTeX}$ file prepared by the author.